Proceedings of the 7th International Symposium on Cavitation
CAV2009 – Paper No. 99
August 17-22, 2009, Ann Arbor, Michigan, USA

MULTIPHASE FLOW ANALYSIS OF CYLINDER USING A NEW CAVITATION MODEL

Cong-Tu Ha
School of Mechanical Engineering
Pusan National University
Busan 609-735, Korea

Warn-Gyu Park
School of Mechanical Engineering
Pusan National University
Busan 609-735, Korea

Charles L. Merkle
School of Aeronautics and Astronautics
Purdue University
West Lafayette, IN 47907-2045, U.S.A.

ABSTRACT

Cavitating flow simulation is of practical importance for many engineering systems, such as marine propellers, pump impellers, nozzles, injectors, torpedoes, etc. The present work is to test a new cavitation model. The governing equation is the Navier-Stokes equation based on an homogeneous mixture model. The solver employs an implicit preconditioning algorithm in curvilinear coordinates. The computations have been carried out for the cylinders with 0-, 1/2- and 1-caliber forebody and then compared with experiments and other numerical results. Fairly good agreement with experiments and numerical results has been achieved.

INTRODUCTION

Cavitation generally occurs if the pressure in some region of liquid flow drops below the vapor pressure and, consequently, the liquid is vaporized and replaced by a 'cavity.' Cavitating flow is often observed in various propulsion systems and high-speed underwater objects, such as marine propellers, impellers of turbomachinery, hydrofoils, nozzles, injectors and torpedoes. This phenomenon usually causes severe noise, vibration and erosion. Even though cavitating flow is a complex phenomenon which has not been completely modeled, a lot of attention has been gathered in the CFD community as methodologies for single-phase flow has matured. Solutions of multiphase flows by CFD methods can be categorized into three groups: The first group uses a single continuity equation [1], [2]. This method is known to be unable to distinguish between condensable and non-condensable gas [3]. The next group solves separate continuity equations for the liquid and vapor phases by adding source terms of mass transfer between phase changes [3]-[9]. These models are usually called homogeneous mixture models because the liquid-gas interface is assumed to be in dynamical and thermal equilibrium and, consequently, mixture momentum and energy equations are used. The final group incorporated full two-fluid modeling, wherein separate momentum and energy equations are employed for the liquid and the vapor phases [10], [11]. This method is widely used in nuclear engineering.

The objective of the present work is to evaluate a new cavitation model that is developed by Merkle et al., [12] (herein referred to as 'Model I'). Two other cavitation models, the first one given by Kunz et al., [4] ('Model II') and the other given by Yuan et al., [13] ('Model III') are also coupled to the transport equations and used for comparison. In the following sections, the governing equations, cavitation models, and numerical method are briefly presented. The cavitation code using Model I is then validated for several axisymmetric bodies under many flow conditions. Finally, the results of the new cavitation model are compared to those of Models II and III to further support its validity.

MATHEMATICAL AND NUMERICAL DESCRIPTIONS

Governing equations

The two-phase preconditioned equations which are normalized with the liquid density, liquid viscosity, free stream velocity, and the characteristic length of the body are written in generalized curvilinear coordinates as follows [4]:

$$\Gamma_e \frac{\partial \hat{Q}}{\partial t} + \Gamma \frac{\partial \hat{Q}}{\partial \tau} + \frac{\partial (\hat{E} - \hat{E}^v)}{\partial \xi} + \frac{\partial (\hat{F} - \hat{F}^v)}{\partial \eta} + \frac{\partial (\hat{G} - \hat{G}^v)}{\partial \zeta} = \hat{S} \qquad (1)$$

where

$$\hat{Q} = \frac{1}{J}\begin{pmatrix} p \\ u \\ v \\ w \\ \alpha_l \end{pmatrix} \tag{2}$$

The convective flux terms are

$$\hat{E} = \frac{1}{J}\begin{pmatrix} U \\ \rho_m uU + \xi_x p \\ \rho_m vU + \xi_y p \\ \rho_m wU + \xi_z p \\ \alpha_l U \end{pmatrix};\ \hat{F} = \frac{1}{J}\begin{pmatrix} V \\ \rho_m uV + \eta_x p \\ \rho_m vV + \eta_y p \\ \rho_m wV + \eta_z p \\ \alpha_l V \end{pmatrix};$$

$$\hat{G} = \frac{1}{J}\begin{pmatrix} W \\ \rho_m uW + \zeta_x p \\ \rho_m vW + \zeta_y p \\ \rho_m wW + \zeta_z p \\ \alpha_l W \end{pmatrix} \tag{3}$$

The contravariant velocities are given by

$$U = \xi_t + \xi_x u + \xi_y v + \xi_z w;\quad V = \eta_t + \eta_x u + \eta_y v + \eta_z w;$$
$$W = \zeta_t + \zeta_x u + \zeta_y v + \zeta_z w \tag{4}$$

The viscous terms are

$$\hat{E}^v = \frac{(\mu_t + \mu_m)}{J\,Re_\infty}\begin{pmatrix} 0 \\ (\nabla\xi.\nabla\xi)\partial_\xi u + (\nabla\xi.\nabla\eta)\partial_\eta u + (\nabla\xi.\nabla\zeta)\partial_\zeta u \\ (\nabla\xi.\nabla\xi)\partial_\xi v + (\nabla\xi.\nabla\eta)\partial_\eta v + (\nabla\xi.\nabla\zeta)\partial_\zeta v \\ (\nabla\xi.\nabla\xi)\partial_\xi w + (\nabla\xi.\nabla\eta)\partial_\eta w + (\nabla\xi.\nabla\zeta)\partial_\zeta w \\ 0 \end{pmatrix}$$

$$\hat{F}^v = \frac{(\mu_t + \mu_m)}{J\,Re_\infty}\begin{pmatrix} 0 \\ (\nabla\eta.\nabla\xi)\partial_\xi u + (\nabla\eta.\nabla\eta)\partial_\eta u + (\nabla\eta.\nabla\zeta)\partial_\zeta u \\ (\nabla\eta.\nabla\xi)\partial_\xi v + (\nabla\eta.\nabla\eta)\partial_\eta v + (\nabla\eta.\nabla\zeta)\partial_\zeta v \\ (\nabla\eta.\nabla\xi)\partial_\xi w + (\nabla\eta.\nabla\eta)\partial_\eta w + (\nabla\eta.\nabla\zeta)\partial_\zeta w \\ 0 \end{pmatrix}$$

$$\hat{G}^v = \frac{(\mu_t + \mu_m)}{J\,Re_\infty}\begin{pmatrix} 0 \\ (\nabla\zeta.\nabla\xi)\partial_\xi u + (\nabla\zeta.\nabla\eta)\partial_\eta u + (\nabla\zeta.\nabla\zeta)\partial_\zeta u \\ (\nabla\zeta.\nabla\xi)\partial_\xi v + (\nabla\zeta.\nabla\eta)\partial_\eta v + (\nabla\zeta.\nabla\zeta)\partial_\zeta v \\ (\nabla\zeta.\nabla\xi)\partial_\xi w + (\nabla\zeta.\nabla\eta)\partial_\eta w + (\nabla\zeta.\nabla\zeta)\partial_\zeta w \\ 0 \end{pmatrix} \tag{5}$$

The source term, $\hat{S}$, is given as follows:

$$\hat{S} = \frac{1}{J}\left\{(\dot{m}^+ + \dot{m}^-)\left(\frac{1}{\rho_l} - \frac{1}{\rho_v}\right),\ 0,\ 0,\ 0,\ (\dot{m}^+ + \dot{m}^-)\frac{1}{\rho_l}\right\}^T \tag{6}$$

The density and viscosity of the liquid and vapor are assumed to be constant. The mixture density and viscosity of the liquid and vapor are defined as

$$\rho_m = \alpha_l \rho_l + \alpha_v \rho_v \tag{7}$$

$$\mu_m = \alpha_l \mu_l + \alpha_v \mu_v \tag{8}$$

The pre-conditioning matrix and flux Jacobian matrix are given by

$$\Gamma = \begin{pmatrix} \left(\frac{1}{\rho_m \beta^2}\right) & 0 & 0 & 0 & 0 \\ 0 & \rho_m & 0 & 0 & u\Delta\rho_l \\ 0 & 0 & \rho_m & 0 & v\Delta\rho_l \\ 0 & 0 & 0 & \rho_m & w\Delta\rho_l \\ \left(\frac{\alpha_l}{\rho_m \beta^2}\right) & 0 & 0 & 0 & 1 \end{pmatrix} \tag{9}$$

$$\Gamma_e = \begin{pmatrix} 0 & 0 & 0 & 0 & 0 \\ 0 & \rho_m & 0 & 0 & u\Delta\rho_l \\ 0 & 0 & \rho_m & 0 & v\Delta\rho_l \\ 0 & 0 & 0 & \rho_m & w\Delta\rho_l \\ 0 & 0 & 0 & 0 & 1 \end{pmatrix} \tag{10}$$

For the system closure, a two-equation k-ε low Reynolds number given by Chien [15] with standard wall functions is adopted in this study

Cavitation models

Cavitation Model I (Merkle at el. 2006)

The evaporation and condensation rates are given as follows

$$\dot{m}^- = -k_v \frac{\rho_v \alpha_l}{t_\infty} \min\left\{1, \max\left(\frac{(p_v - p)}{k_p p_v}, 0\right)\right\}$$
$$\dot{m}^+ = k_l \frac{\rho_v \alpha_v}{t_\infty} \min\left\{1, \max\left(\frac{(p - p_v)}{k_p p_v}, 0\right)\right\} \tag{11}$$

In this model, a ramping function is defined as

$$f = \min\left\{1, \max\left(\frac{(p_v - p)}{k_p p_v}, 0\right)\right\} \tag{12}$$

which is only to ensure the stability of the numerical scheme. Hence, the factor k_p should be as small as possible so that the scaling constants are the only main parameters which control phase changes.

Cavitation Model II (Kunz et al. 2000)

The evaporation and condensation rates are given as follows

$$\dot{m}^- = \frac{C_{dest}\rho_v \alpha_l \min[0, p - p_v]}{\left(\rho_l U_\infty^2 / 2\right) t_\infty}$$
$$\dot{m}^+ = \frac{C_{prod}\rho_v \alpha_l^2 (1 - \alpha_l)}{t_\infty} \tag{13}$$

The empirical constants used in this study are C_{dest}=1000 and C_{prod}=10.

Cavitation Model III – Bubble dynamics (Yuan et al. 2003)

In this model, the cavity is assumed to consist of small spherical bubbles. The effects of bubble acceleration, viscous, and surface tension are neglected. The bubble growth/collapse rates are given in the simple Reyleigh-Plesset relation as follows

$$\dot{m}^- = \begin{cases} -\rho_v L(4\pi N)^{1/3}(3\alpha_v)^{2/3}\sqrt{\frac{2}{3}\frac{|p_v - p|}{\rho_l}} & \text{when } p \le p_v \text{ and } \alpha_v < 1 \\ 0 & \text{when } p > p_v \text{ or } \alpha_v = 1 \end{cases}$$

$$\dot{m}^+ = \begin{cases} \rho_v L(4\pi N)^{1/3}(3\alpha_v)^{2/3}\sqrt{\frac{2}{3}\frac{|p_v - p|}{\rho_l}} & \text{when } p > p_v \\ 0 & \text{when } p \le p_v \end{cases} \tag{14}$$

where N, the number of bubbles per unit volume ($1/m^3$), can typically be determined by numerical experiments. A constant value of $5.0x10^8$ bubbles/m^3 is adopted in this study.

Numerical method

The preconditioning system (1) can be written in the finite difference form as follows

$$\Gamma_e \frac{3\Delta\hat{Q}^{n+1,k}}{2\Delta t} + \Gamma\frac{\Delta\hat{Q}^{n+1,k}}{\Delta\tau} + \left(\frac{\partial A}{\partial\xi} + \frac{\partial B}{\partial\eta} + \frac{\partial C}{\partial\zeta} - \frac{\partial A^v}{\partial\xi} - \frac{\partial B^v}{\partial\eta} - \frac{\partial C^v}{\partial\zeta}\right)^{n+1,k}\Delta\hat{Q}^{n+1,k}$$
$$= -\Gamma_e \frac{3\hat{Q}^{n+1,k} - 4\hat{Q}^n + \hat{Q}^{n-1}_{i,j}}{2\Delta t} - \left(\frac{\partial\hat{E}}{\partial\xi} + \frac{\partial\hat{F}}{\partial\eta} + \frac{\partial\hat{G}}{\partial\eta} - \frac{\partial\hat{E}^v}{\partial\xi} - \frac{\partial\hat{F}^v}{\partial\eta} - \frac{\partial\hat{G}^v}{\partial\eta} - \hat{S}\right)^{n+1,k} \tag{15}$$

where $\Delta\hat{Q}^{n+1,k} = \hat{Q}^{n+1,k+1} - \hat{Q}^{n+1,k}$; n represents the index of the physical-time level and *k* is the index of the pseudo-time level.

Equation (15) was solved by Beam-Warming scheme after discretizing the spatial derivatives with central differences.

Boundary conditions

The boundary conditions used in the present simulations includes inflow, outflow, no-slip, and symmetric boundary conditions. At the inlet, the velocity and liquid fraction are imposed and the pressure is extrapolated from the interior points. At the downstream, pressure is imposed while the other variables are extrapolated. At the wall, the velocity is zero while the other variables are extrapolated from the interior points. Along the centerline, all variables are extrapolated from the interior points.

RESULT AND DISSCUSION

Three configurations of 0-, 1/2-, and 1-caliber cylinder, as depicted in Figure 1, were used to validate the cavitation model I. A grid of dimension of 199x80x37 is used for 0-caliber cylinder while a grid of dimension of 120x132x37 is used for 1/2, and 1-caliber cylinder configurations. All grids are clustered in the normal direction near the body surface and in the spanwise direction. A nominal density ratio of 1000 is assigned. A Reynolds number of $1.46x10^5$, based on the diameter of the cylinder, is used for the simulations of 0-caliber cylinder and a value of Reynolds number $1.36x10^5$ is used for simulations of 1/2- and 1-caliber cylinders. Before validating the new model for all configurations, several simulations were done to check its stability and to set the values of the constants k_v, k_l and k_p. The scaling constants k_v of 100.0 and a ratio k_v/k_l of 15.0, and k_p of 0.02 are then used for the computations presented in this section.

Figure 2 shows the time-averaged surface pressure distribution for the 0-caliber cylinder using model I at cavitation numbers of 0.3 and 0.5. Good agreement was obtained in the body of the vapor cavity, compared with the data [16] and Owis and Neyfeh's computations [17] except that at the head of the cylinder, the obtained results are a little overestimated and at the tail of the vapor cavity the results are somewhat underestimated. The discrepancy may be related to several reasons. First, it may be due to the inaccurate estimation of the turbulent viscosity in the region where large flow gradients exist such as at the sharp corner. Further discussion on this limitation of the standard k-ε model can be referred in Refs. [14, 18]. In addition, the fluid compressibility and the cavitation-induced turbulence effects have not been taken into account in the present model, which results in the fact that the model cannot well reflect physical phenomenon in highly-compressible mixture regions. Other reasons may come from the accuracy of cavitation models as well as the grid resolution.

As mentioned above, the scaling constants in Model I, are the main parameters that control how fast a phase change occurs and how much of the new phase can be produced. Figure 3 shows the flow fields and vapor fraction contours for a cavitation number of 0.5 about a 0-caliber cylinder for three sets of scaling constants at a particular dimensionless time of 7.0. Here, the scaling constant k_v holds a value of 100.0 while the ratios k_v/k_l are 0.1, 1.0, and 15.0. In these cases, the same rate of vapor production is applied, resulting in the same cavity length. However, the effect of rate of liquid production has a strong impact on the flow velocity in the vicinity of the cavitating structures resulting in different cavity-vortex interaction and re-entrant flow. The presence of these acts against the evolution of the cavity. In other situations, the scaling constants were chosen such that the rates of vapor/liquid production are different. Here, the scaling constants k_v are 0.1, 1.0, 10.0, and 100.0 while the ratio k_v/k_l holds a value of 10. As depicted in Figure 4, using different scaling constants leads to changing the vapor volume fraction distribution within the cavity as well as the flow fields. Figure 5 shows the similar contours for Model II using different sets of empirical constants, C_{dest} and C_{prod}. It can be seen that Model II also seems to be sensitive to the empirical constants.

Figure 6 shows the comparison of transient plots of vapor volume fraction contour against those predicted by Model II and Model III. Clearly, the vapor distribution predicted by Mode I at these dimensionless time instants agree very well with those predicted by Model II. With Model III, the re-entrant flow is more prominent. Since there is no difference between growth and collapse of the bubble (Equation 14), Model III produces a larger amount of vapor in the low pressure region compared to Models I and II resulting in changes in the density of the mixture and hence changes in pressure gradients. An

increase in adverse pressure gradient near the closure region of the cavity has a direct impact on the development of the re-entrant motion and causes the cavity to roll up and separate.

Figures 7 and 8 present the time-averaged surface pressure distribution for the 1/2- and 1-caliber cylinders using Model I at different cavitation numbers. For both configurations, the results well capture the cavity pressure distribution and cavity size.

The comparisons among the Model I, Model II, and Model III are presented in Figures 9 and 10 for the flow over a 1/2 caliber cylinder at two cavitation numbers of 0.2 and 0.4, respectively, and in Figures 11 and 12 for the flow over a 1-caliber cylinder at two cavitation numbers of 0.24 and 0.32, respectively. The computational results of Models I and II are in close agreement with each other and with data while the cavity length obtained by Model III is slightly smaller than the one obtained by Model I and II. It should be noted that the number density, N, may play the key control in Model III and it should not be kept constant throughout the whole domain. Keeping this number as a constant may not be sufficient to accurately model the cavitation dynamics, as discussed in Ref. [18].

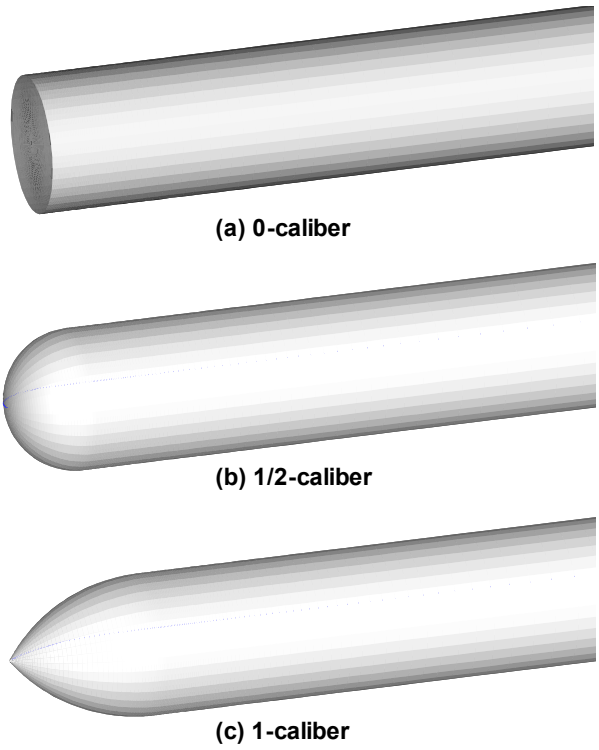

Figure 1: Configurations of axisymmetric cylinder

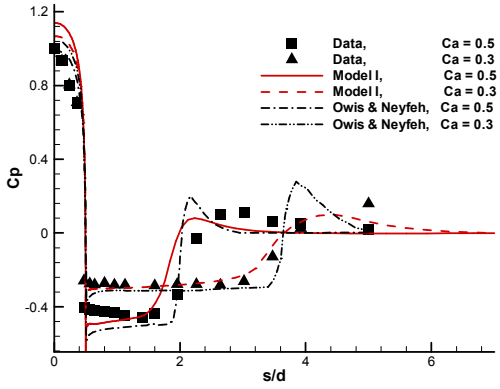

Figure 2: Comparison of time-averaged surface pressures for flow over a 0-caliber cylinder

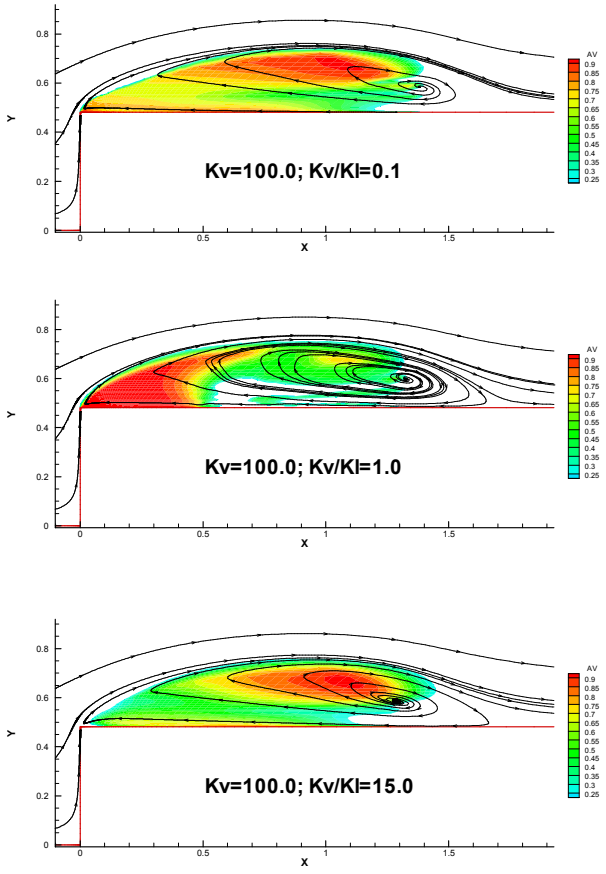

Figure 3: Vapor fraction contour and flow field for flow over a 0-caliber cylinder at Ca=0.5; t=7.0 (Model I)

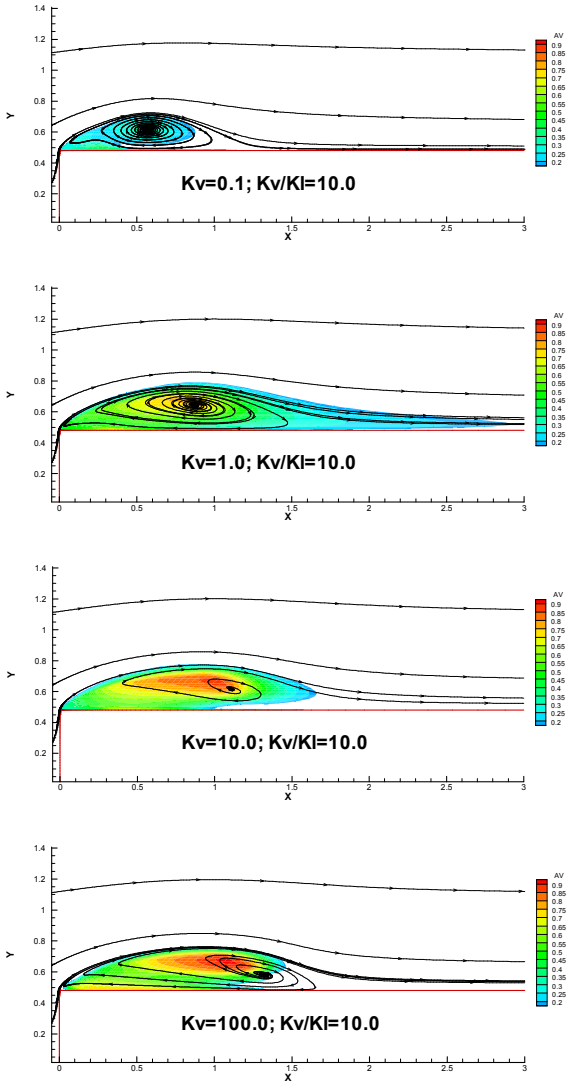

Figure 4: Vapor fraction contour and flow field for flow over a 0-caliber cylinder at Ca=0.5; t=7.0 (Model I)

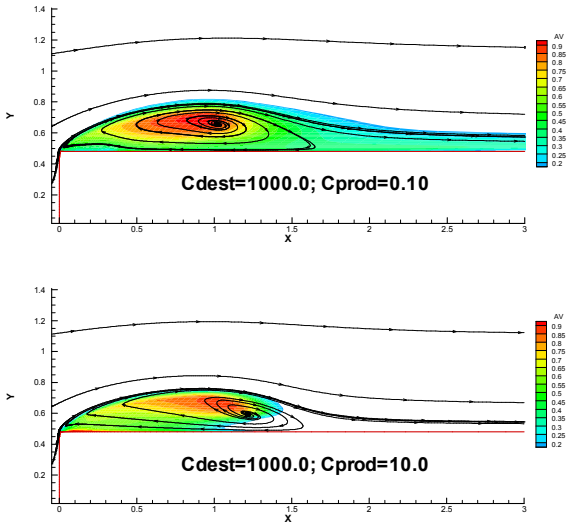

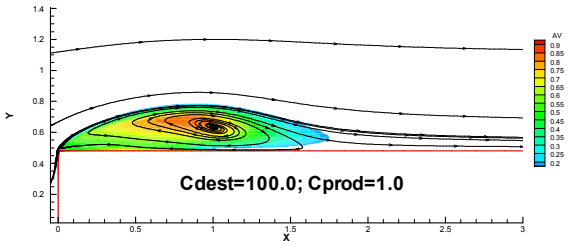

Figure 5: Vapor fraction contour and flow field for flow over a 0-caliber cylinder at Ca=0.5; t=6.5 (Mode II)

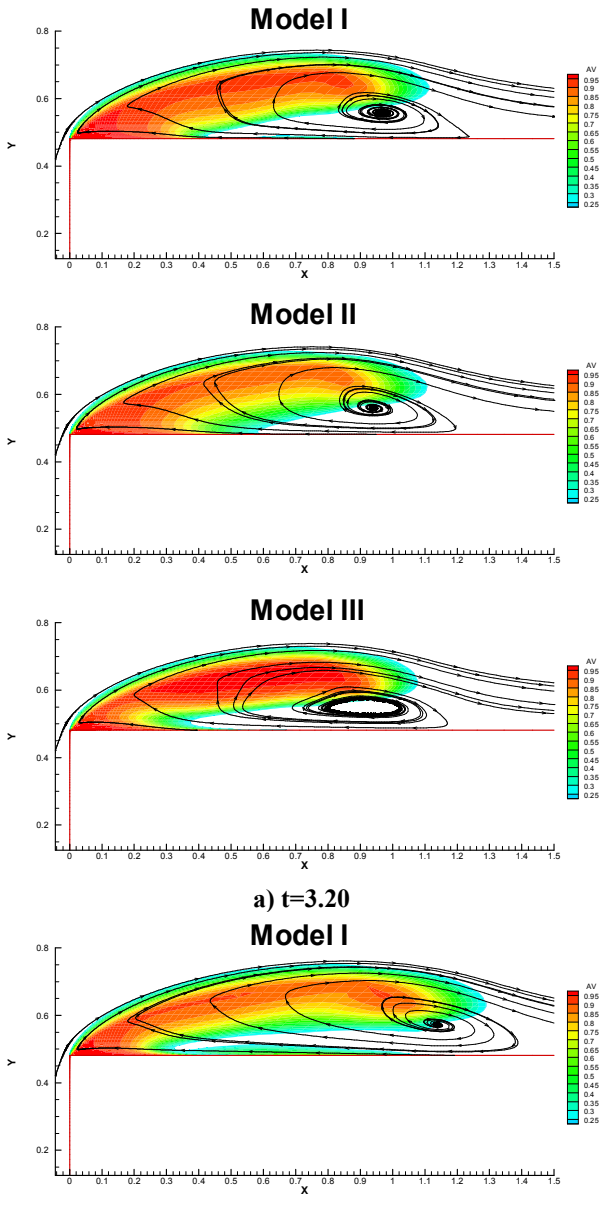

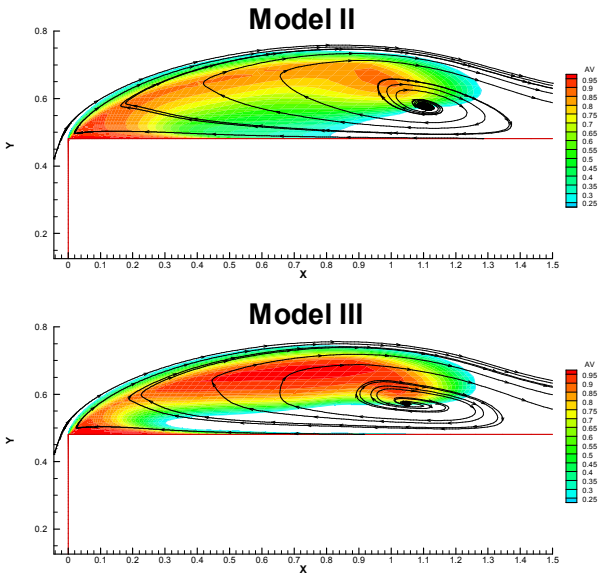

b) =4.47

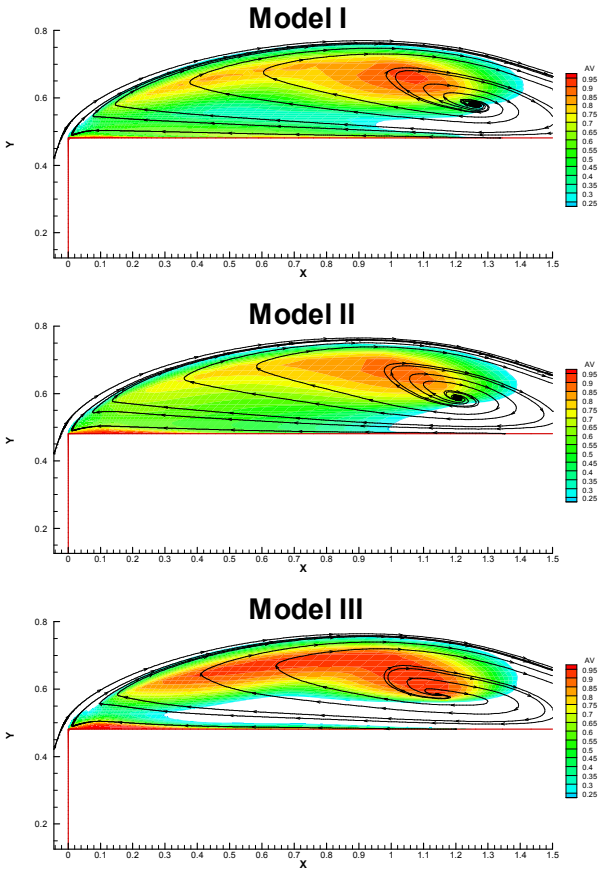

c) t=6.04

Figure 6: Comparison of transient evolution of vapor volume fraction and flow field for flow over 0-caliber cylinder at Ca=0.5

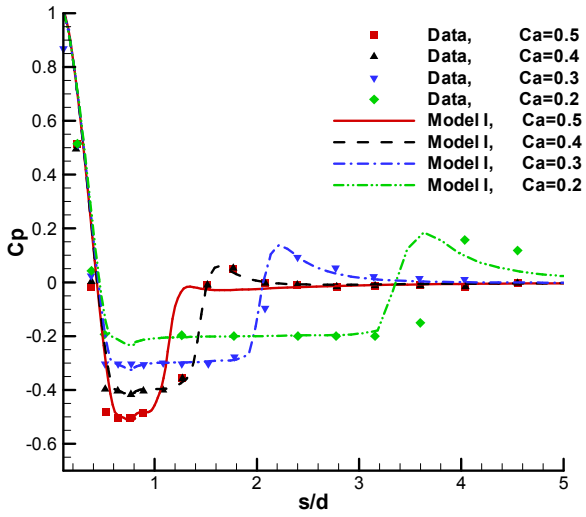

Figure 7: Comparison of time-averaged surface pressures for flow over 1/2-caliber cylinder

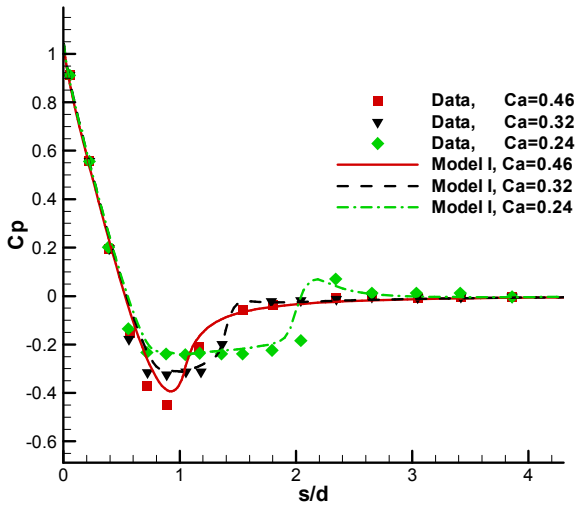

Figure 8: Comparison of the time-averaged surface pressure for flow over 1-caliber cylinder

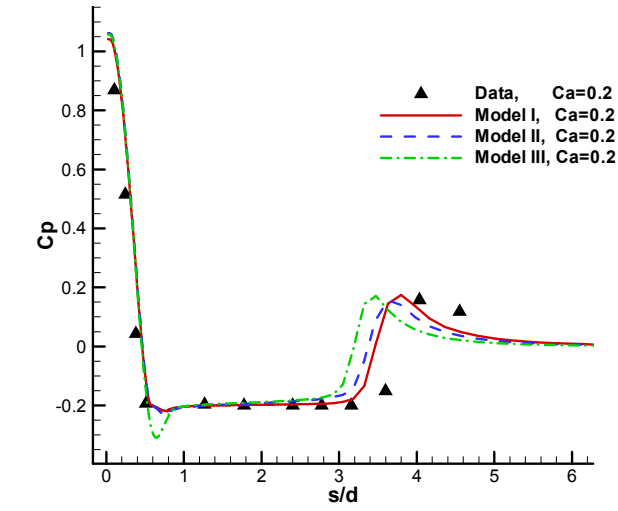

(a)

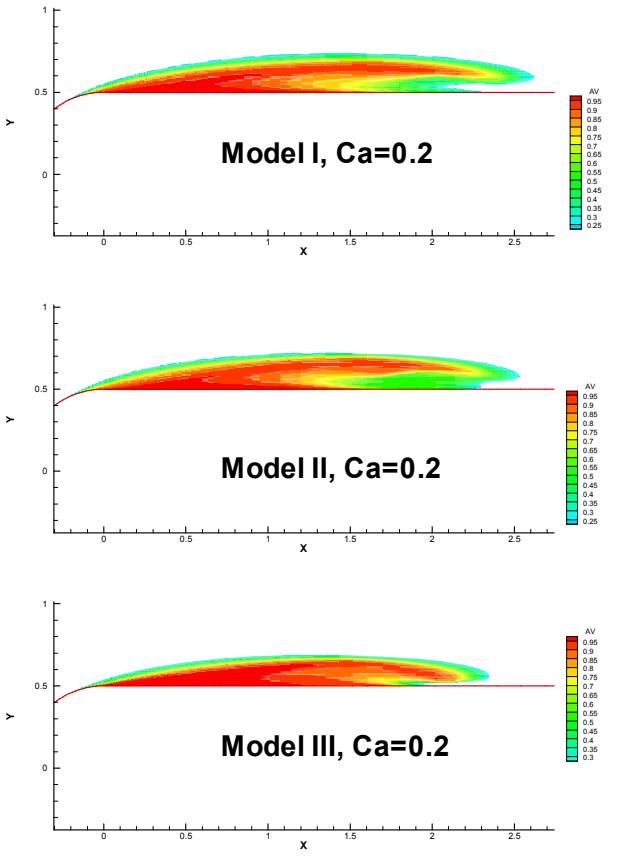

(b)

Figure 9: (a) Time-averaged surface pressures and **(b)** predicted vapor volume fraction contour for 1/2-caliber cylinder at t=47.1

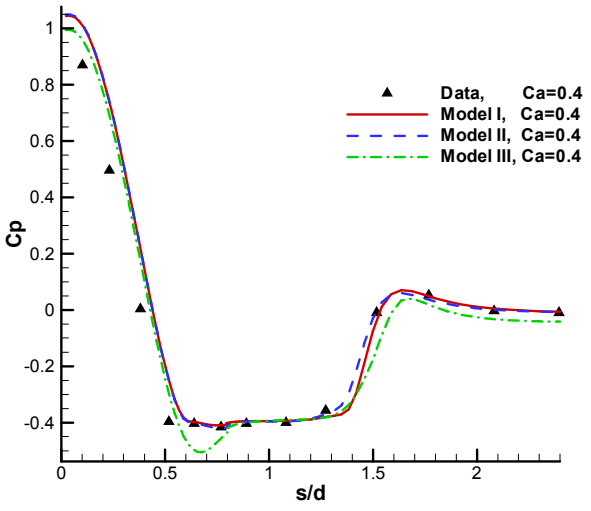

(a)

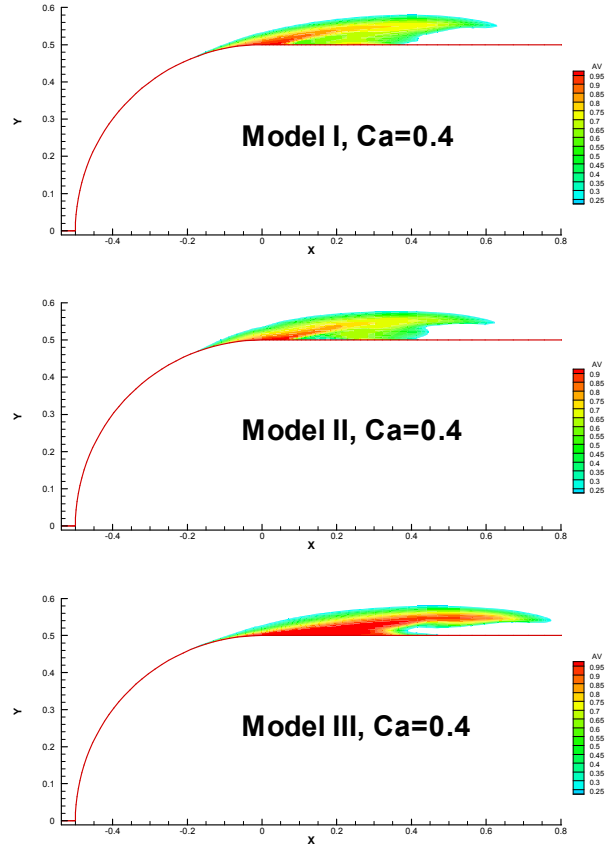

(b)

Figure 10: (a) Time-averaged surface pressures and **(b)** predicted vapor volume fraction contours for 1/2-caliber cylinder at t=24.3

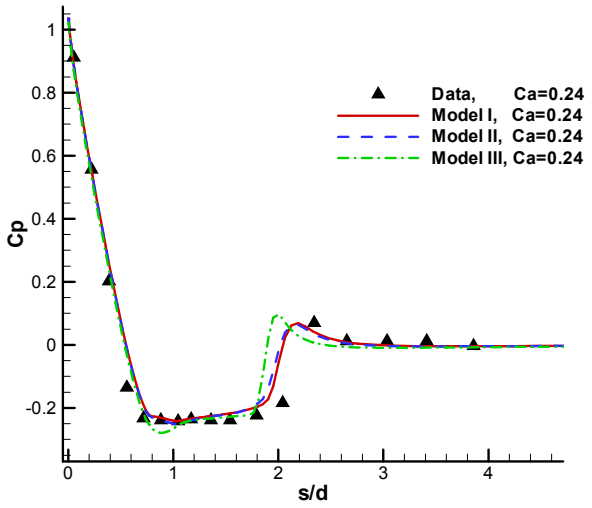

(a)

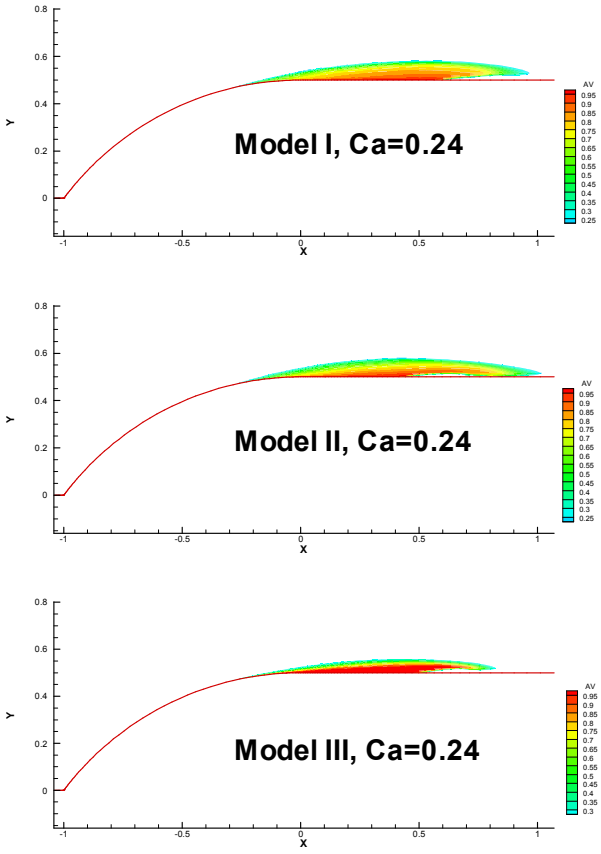

(b)

Figure 11: (a) Time-averaged surface pressures and **(b)** predicted vapor volume fraction contours for 1-caliber cylinder at t=50.3

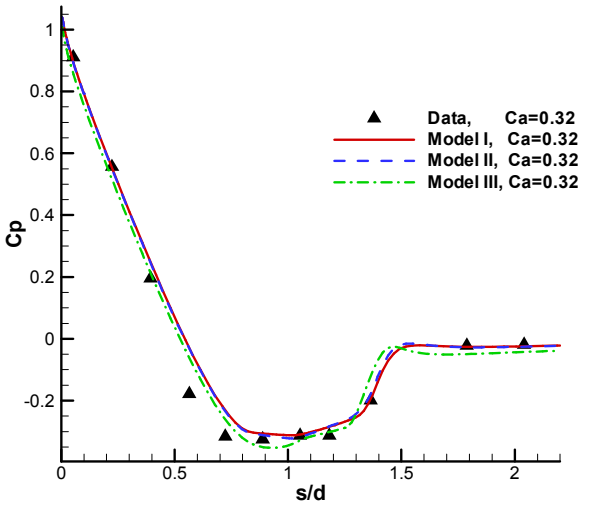

(a)

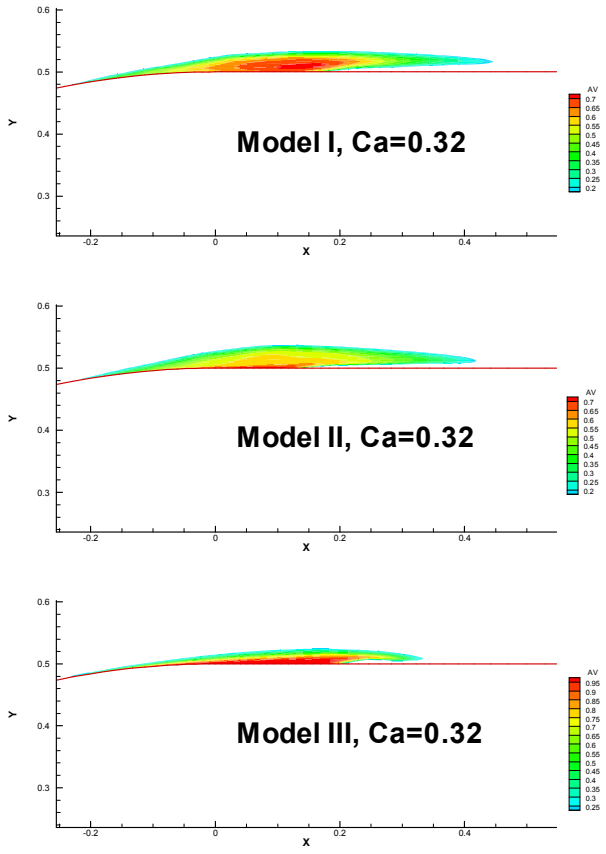

(b)

Figure 12: (a) Time-averaged surface pressures and **(b)** predicted vapor volume fraction contours for 1-caliber cylinder at t=45.0

CONCLUSIONS

A new cavitation model has successfully been validated for different configurations under many flow conditions. The model works stably. Like existing models, the new cavitation model requires mass transfer model constants which play the key role of controlling the mechanism of phase change. These constants can easily be determined by numerical experiments. Future work will focus on validation for more complex configurations and take account into compressible fluids as well as cavitation-induced turbulence effects.

ACKNOWLEDGMENTS

The authors gratefully acknowledge the support from Underwater Vehicle Research Center (UVRC), Agency for Defense Development (ADD), and Defense Acquisition Program Administration (DAPA) of Korea.

NOMENCLATURE

Symbols

A, B, C	convective Jacobian matrix
A^v, B^v, C^v	viscous Jacobian matrix
Ca	cavitation number, $Ca = \frac{p_\infty - p_v}{\frac{1}{2}\rho_\infty U_\infty^2}$
C_{dest}, C_{prod}	mass transfer model constants
$\hat{E}, \hat{F}, \hat{G}, \hat{E}^v, \hat{F}^v, \hat{G}^v, \hat{Q}, \hat{S}$	flux vectors in ξ, η, and ζ directions, solution vector, source vector
f	ramping function
J	Jacobian of the transformation
k	scaling constant
L	length scale
$\dot{m}^-$, $\dot{m}^+$	evaporation and condensation rates
N	bubble number density
p	pressure
Re_∞	Reynolds number, $Re_\infty = \frac{U_\infty L \rho_l}{\mu_l}$
t, t_∞	time, characteristic time, $t_\infty = L/U_\infty$
u, v, w	Cartesian velocity components
U, V, W	contravariant velocities
α	volume fraction
β	preconditioning parameter
Γ_e, Γ	flux Jacobian matrix, precondition matrix
μ	dynamic viscosity
ρ	density
$\Delta\rho_l$	density difference, $\Delta\rho_l = \rho_l - \rho_v$
τ	pseudo time, stress

Subscripts

L	liquid
T	turbulent
V	vapor
∞	free stream value

REFERENCES

[1] Reboud, J. L., Delannoy, Y., 1994, " Two-phase flow modeling of unsteady cavitation," *Proc. of 2nd International Symposium on Cavitation,* Tokyo, Japan, 39-44.

[2] Song, C., He, J., 1998, "Numerical simulation of cavitating flows by single-phase flow approach," *Proc. of 3rd International Symposium on Cavitation,* Grenoble, France, 295-300.

[3] Kunz, R. F., Lindau, J. W., Billet M. L., and Stinebring D. R., "Multiphase CFD modeling of Developed and Supercavitaing Flows," *Proceedings of the Von Karman Institute Special Course on Supercavitating Flows*, 12-16 February 2001, Rhode-Saint-Genese, Belgium.

[4] Kunz, R. F., Boger, D. A., Stinebring, D. R, Chyczewski, T. S. , Lindau, J. W. , Gibeling H. J., Venkateswaran, S, Govindan, T. R., 2000, "A preconditioned Navier–Stokes method for two-phase flows with application to cavitation prediction," *Computers and Fluids*, Vol 29, pp. 849.

[5] Merkle, C. L., Feng, J. Z., Buelow, P. E. O., 1998, "Computational Modeling of the Dynamics of Sheet Cavitation", *Proc. of the 3rd International Symposium on Cavitation,* Grenoble, France, 307-311.

[6] Kunz, R. F., Boger, D. A., Stinebring, D. R, Chyczewski, T. S. , Lindau, J. W. , Gibeling H. J., Venkateswaran, S, Govindan, T. R., 2000, "A preconditioned Navier–Stokes method for two-phase flows with application to cavitation prediction", *Computers and Fluids,* 29, 849-875.

[7] Ahuja, V., Hosangadi, A., Arunajatesan, S., 2001, "Simulation of Cavitating Flow Using Hybrid Unstructured Meshes", *Jounal of Fluids Engineering,* 123, 331-340.

[8] Shin, B. R., Itohagi, T., 1998, "A numerical study of unsteady cavitaing flows," *Proc. of the 3rd International Symposium on Cavitation,* Grenoble, France, 301-306.

[9] W. Yuan, H.G. Schnerr, 2003, "Numerical simulation of two-phase flow in injection nozzles: interaction of cavitation and external jet formation", *Jounal of Fluids Engineering,* 125, 963–969.

[10] Grogger, H. A., Alajbegovic, A., 1998, "Calculation of the cavitating flow in venture geometries using two fluid model," *ASME Paper FEDSM 98-5295*.

[11] Staedkte, H., Deconinck, H., and Romenski, E., 2005, "Advanced three-dimensional two-phase flow simulation tools for application reactor safety(ASTAR)," *Nuclear Engineering and Design,* 235, 379-400.

[12] Merkle, C.L., Li, D., and Venkateswaran, S., 2006, "Multi-Disciplinary computational analysis in propulsion", AIAA Paper 2006-4575.

[13] Yuan, W., Schnerr, H. G., 2003, "Numerical simulation of two-phase flow in injection nozzles: interaction of cavitation and external jet formation," *Jounal of Fluids Engineering* 125, 963–969.

[14] Payne, J. L. et al. "A Comparison of Turbulence Models for a Supersonic Jet in Transonic Crossflow", *AIAA 2001-1048,*39th AIAA aerospace Sciences Meeting & Exhibit.

[15] Chien K. Y., 1982, "Prediction of Change and Boundary Layer Flows with a Low-Reynolds-Number Turbulence Model," *AIAA Journal*, Vol.22, pp. 33-38.

[16] Rouse H., McNown J.S., "Cavitation and Pressure Distribution", *Head Forms at Zero Angle of Yaw*, Stud. Engrg., vol. 32, State University of Iowa, 1948.

[17] Owis F. M., Nayfeh A. H., 2003, "Computational of Compressible Multiphase Flow Over the Cavitating High-Speed Torpedo", *Jounal of Fluids Engineering*, Vol 125, 459-468.

[18] Srinivasan, V., Salazar, A. J., Saito, K., 2009, "Numerical simulation of cavitation dynamics using a cavitation-induced-momentum-defect (CIMD) correction approach," *Applied Mathematical Modelling* 33, 1529–1559.

[19] Kunz, R., Boger, D., Chyczewski, T., Stinebring, D., Gibeling, H., 1999, "Multi-phase CFD analysis of natural and ventilated cavitation about submerged bodies", *ASME FEDSM* 99-7364, San Francisco.

[20] Venkateswarn, S., Lindau, J. W., Kunz, R.F., Merkle, C. L., 2001, "Preconditioning Algorithms for Computation of Multi-Phase Mixture Flows", *AIAA 39th Aerospace Sciences Meeting & Exhibit*, AIAA Paper 2001-0279.